Towards a Micromechanics Model for Continuous Carbon Fiber Composite 3D Printed Parts

Adnan Abdullahi, Immanuella Kankam, Abhay Singh Gahloth, Bhavya Arora, Ankit Agarwal, Trevor Eppley, Ziyad Salti, Derek Goss, Raghav Sharma, Dhruv Bhate*
Ira A. Fulton Schools of Engineering, Arizona State University, Tempe, AZ 85281
*Corresponding Author: dhruv.bhate@asu.edu

Abstract

Material extrusion is transitioning from a technology mainly for rapid prototyping to one that is increasingly finding use in manufacturing functional parts. Of particular interest in this regard is the reinforcement of extruded parts with Continuous Carbon Fiber (CCF). However, predicting the effective properties of 3D printed composite parts presents a unique challenge because of the strong effects of meso-structure on the mechanical behavior of printed parts. This work aims to develop a mathematical model that would enable such a prediction of behavior by incorporating the rule of mixtures commonly used in micromechanics modeling. Results from tensile tests on composite specimens with varying volume fractions produced from a blend of onyx (nylon and chopped carbon fiber) and CCF are reported. Volume fractions are varied through a range of factors including the layers with fiber, the distribution of fiber within layers and the angle of the fibers relative to the loading direction, though findings suggest that this has no significant influence on the model itself, and that volume fraction is a sufficient parameter. The predictive ability of the micromechanics model is put to the test for composite honeycombs under compression, and a wide discrepancy between model and experimental result is demonstrated, demonstrating the limitations of such a model and suggesting pathways for improvement.

Keywords

3D Printing, Composite, Carbon Fiber, Micromechanics, Additive Manufacturing, Modeling

Introduction

Over the years, material extrusion has slowly evolved from being the preferred technology for rapid production of prototype parts to a technology that is, in its own right, capable of producing functional parts. This has partly been as a result of development of novel high performance thermoplastics such as ULTEM (PEI), that can meet the design requirements imposed by industry users of the technology, and partly due to an overall improvement in the material extrusion process. Most relevant to this work, is the development of printing technologies that allow for printing of continuous fiber reinforced components. Continuous fiber reinforced components are made possible by a variation of the Material Extrusion process that allows for the combination of varying types of reinforced fibers with conventional polymers to produce parts that have been shown to have properties comparable to aluminum [1,2]. There are numerous ways to achieve integration of fiber into parts. When continuous fiber is the reinforcement material in question, Prüß et al. [3], propose that three methods are most favorable: (i) embedding before the printing process - this involves , incorporation of the fiber before the printing process, achieved normally with filaments that are by themselves composites; (ii) embedding in the printing head-which involves the

combination of two materials/filaments as they pass through a single extruder, and, (iii) embedding in the component itself. The latter case was the method employed for this work and involved using the commercial MarkForged Mark Two 3D printer, which employs two independent extruders, each operating with its own distinct material, with fiber laid after the matrix material [1,3].

The mechanical properties of conventional material extrusion 3D printed parts have been studied in literature [4,5]. Dickson et al. [2] studied nylon composites fabricated with an array of Markforged's fiber reinforcement materials such as CCF, Kevlar and glass fibers, and established comparisons between their mechanical performance. Their work also used the Rule of Mixtures (ROM) approach to estimate the modulus of reinforcing fibers, by performing an inverse calculation using experimentally obtained nylon modulus, total composite strength of the specimens, and the estimated volume fraction of fiber present. Malenka et al. [6] implemented a geometric approach to estimating volume fraction by calculating the volume fraction of the constituent parts of the composite print. Elastic properties of the composite prints were then predicted using a volume averaging stiffness method. More recently, Lozada et al. [1] modified Malenka et al.'s approach, and used the ROM to predict elastic modulus of composite prints made up of nylon matrix and continuous fiber. For simplicity, they assumed isotropy, reducing the compliance matrix to a single value [1]. Their approach achieved good prediction results for low values of carbon fiber volume fraction, but had large deviations at larger fiber volume fractions.

The work in this paper builds on the afore mentioned prior work by attempting to develop a ROM model to predict the tensile properties of continuous carbon reinforced prints. Different from prior work, the paper examines the dependence of the ROM model not just to volume fraction, but how the distribution of fiber may influence properties. Secondly, this work attempts to use this model along with Finite Element Analysis (FEA) to examine its validity when predicting behavior of more complex geometries, in this case of a hexagonal honeycomb, though findings in this latter regard only serve to demonstrate the limitations of the ROM modeling approach.

This paper is divided into four main sections: the first lays out all the methods used to design and fabricate the specimens, the second then discusses the results of the tensile testing conducted on them. Following this, the ROM model is developed, and finally it is applied to the specific case of honeycomb compression, to assess its overall performance. The paper ends with a discussion summarizing key learnings, and identifying future directions.

Design and Fabrication

Specimen Design

The designed geometry for the specimens used in this study was created according to ASTM D638-14 using a Type I geometry [12]. The geometry used in this study, with critical dimensions, are shown in Fig. 1. The specimen geometry was exported as a stereolithography file (STL) and loaded into the *Eiger* 3D printer slicing software package. The Eiger slicing software package is required to not only slice, but also control the placement of the fiber reinforcement amidst other key parameters. This software was the only slicing software that could be used with the accompanying Mark two printer. The length of the specimen in figure 1 differs from the standard type 1 ASTM D638-14 specimen (196.1mm vs 165mm). This was due to a an increase in the grip

section of the specimen to provide for better gripping within the jaws, in keeping with a recommendation that the grip length approach at least 2/3rds of the length of the jaws used to grip the specimen. As we shall show later, these designs failed in the transition from the gauge to the grip section, and therefore may not be ideal candidates for testing.

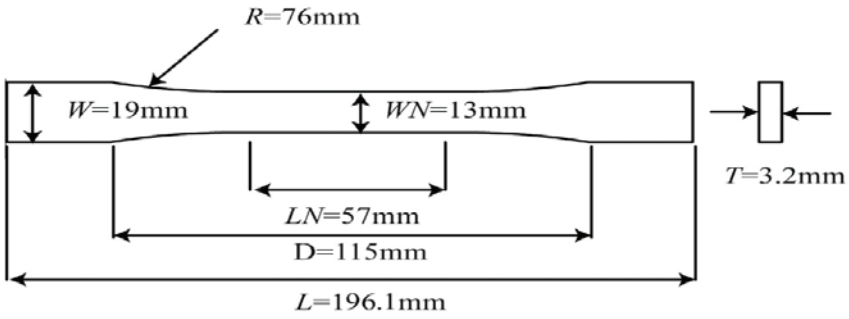

Figure 1. Specimen design geometry used in this study

Fiber Fill Approaches

All specimens produced for this study were fixed as concentric for fiber fill type, and as solid fill for fill pattern. This parameter alongside the layer height were the only parameters that were kept constant for the design process. The dominant feature in composite print design using the *Eiger* platform, is the fiber fill type. Concentric design has the feature of the fiber layers being oriented along the direction of loading, in a repeated fashion, with equal intervals between fiber placement. Figure 2 depicts an *Eiger* generated internal view of the of a concentric infill pattern of fiber for a print specimen. This concentricity feature can be controlled by selecting the number of concentric rings desired for any design.

In addition to defining a concentric fill as shown in Figure 2, it is possible to limit fiber to only certain layers, as shown in Figure 3, where regions in blue correspond to layers with fiber fill, the rest corresponding to layers without fiber. Table 1 list the design details for each individual print sample labelled from 1C-7C. Key terms such as the number of floor and roof layers, are also representative of the top and bottom layers that are by default the matrix of the composite. Likewise, the number of walls is also a parameter that simply defines the number of layers for the matrix along the inner perimeter of the specimen. Layer arrangement in this context simply refers to how the total layers were assigned to be either layers consisting of just onyx, or layers designated to be consisting of mostly fiber, with of course a small narrow infill onyx region as can be seen in figure 2. Hence from the layer arrangement column in Table 1, numbers with the symbol (“) attached to them, for instance 4”, represents fiber layers (in this instance, 4 successive layers with fiber) and the numbers without the symbol (“) attached to them, for instance 1, represents the number of successive matrix layers without fiber (in this instance one matrix layer). Hence for example, specimen 1C with a layer arrangement 1-8”-8-8”-1, would imply after the exclusion of the mandatory roof and floor layers represented by the 1’s at the beginning and the end of the series, means 8 fiber layers followed by 8 layers made up of just onyx, then followed by another 8 fiber layers. All specimens were fabricated on the MarkForged Mark Two 3D printer using MarkForged supplied CCF and Onyx^{TM}, as fiber and matrix, respectively.

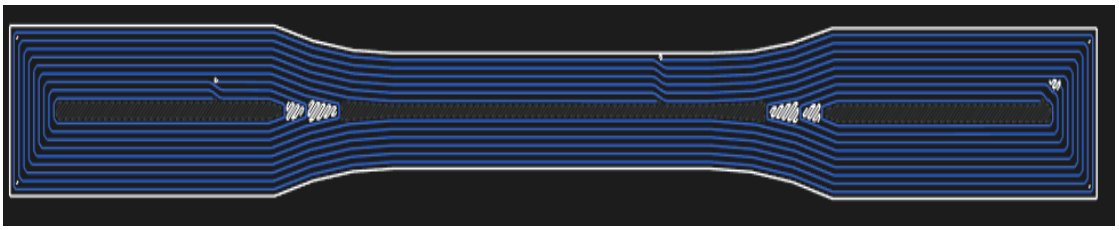

Figure 2. Concentric fill pattern, as generated by the *Eiger* software

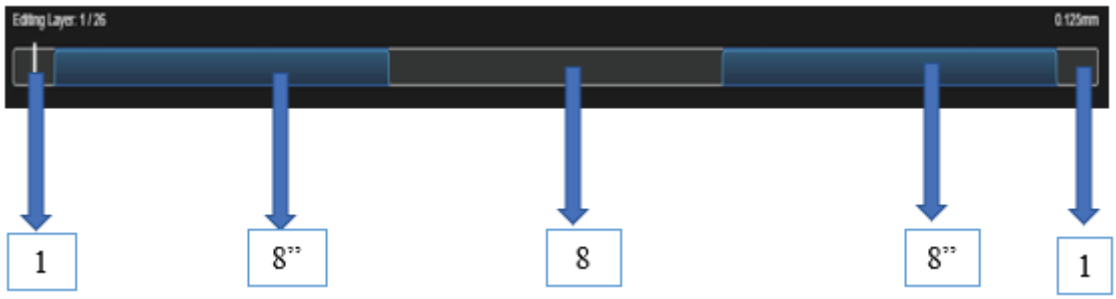

Figure 3. Interpretation of naming convention: blue regions correspond to layers with fiber (and marked with "), transparent regions correspond to layers with only Onyx (and no fiber)

Table 1. Summary of print specimens with naming conventions and volume fractions specified

Sample Number	Layers arrangement	Number of roof and floor layers	Number of walls	Number of total fiber layers	Number of just Onyx layers	Number of concentric rings
1C	1-24"-1	1	1	24	0	1
2C	1-8"-8-8"-1	1	1	16	8	2
3C	1-3"-6-6''-6-3''-1	1	1	12	12	Alternated between 3 and 6 for carbon fiber layers
4C	2-2"-2-2"-2-2"-2-2"-2-2''-2-2"-2	2	1	12	10	6
5C	4-18"-4	4	2	18	0	5
6C	1-8"-8-8"-1	1	1	16	8	6
7C	1-24"-1	1	1	24	0	6

Mechanical Testing

The specimens tested on an Instron 5985 tensile testing frame with 250kN load capacity (and a load cell of the same capacity). A non-contact video extensometer was used to measure strain in the gauge section. Specimens were loaded at a rate of 5mm/min till failure. As shown in Figure 4a, the specimens failed in the transition region from gauge to grip – as a result only modulus values are reported in this work since the strength cannot be confirmed to be reliably representative of the material behavior. Malenka et al. [4] suggest that the failure location for composite prints coincides with the fiber placement start point of the print. As shown in Figure 4b, specimens in this work may have failed at the transition on the account of a change in the layout of fiber and onyx when managing that transition, coincident with several fiber placement starting points in close proximity around that region.

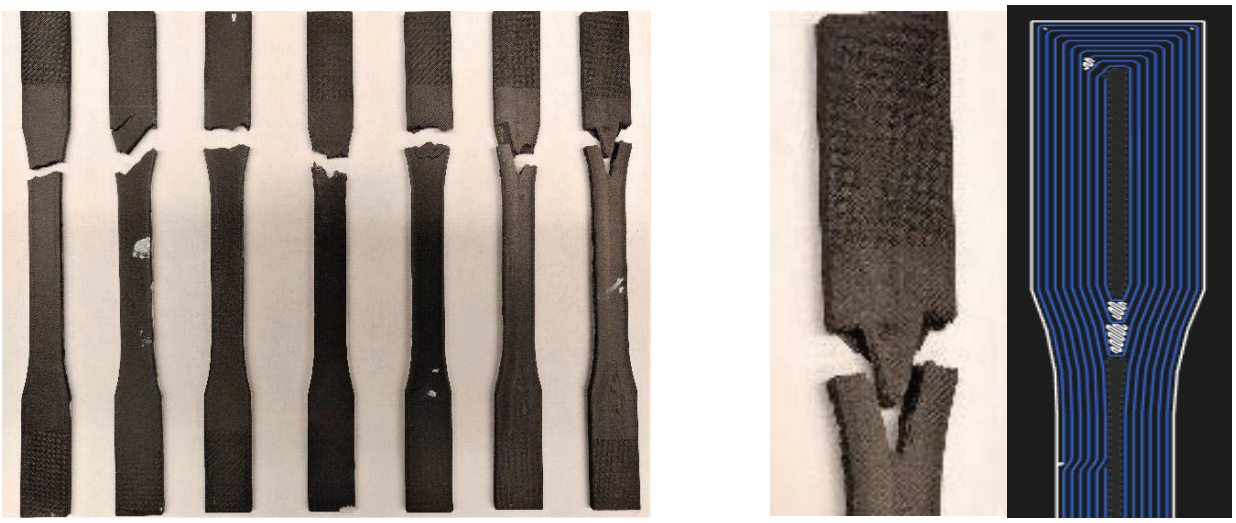

(a) (b)

Figure 4. Failure of print specimens, showing failure in the transition between gauge and grip section – as a result, only elastic modulus values are reported in this work and strength data has been excluded.

Figure 5 shows the results obtained from the tensile tests conducted on the composite print specimens. It can be observed that stress values increased from specimen 1C-7C, in line with expectations. The stress-strain information obtained from the tests were then analyzed in MATLAB© to find Young's modulus values via a regression fit approach to find a fit with an $R^2 > 99\%$. The Young's modulus values obtained are summarized in Table 2. The same methodology was applied to obtain the Young's modulus of a pure onyx ASTM D638-14 type 1 specimen, and a value of 2.493 GPa was obtained. This value is clearly distinctly larger than the value of 1.4 GPa reported by Mark forged material sheet as the Young's modulus for a pure onyx specimen. This difference is potentially due to differences in process parameter settings.

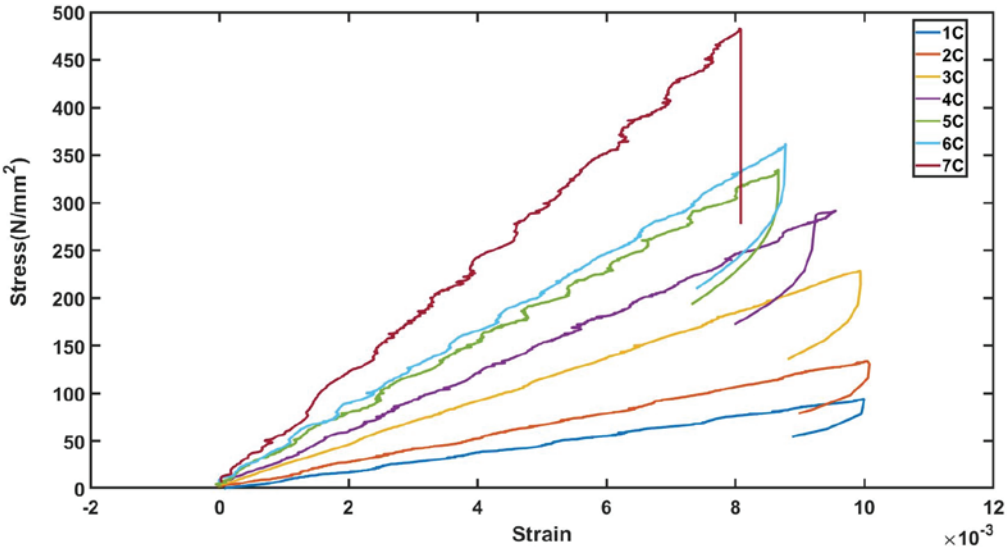

Figure 4. Stress vs Strain for samples 1C-7C

Table 2. Summary of specimens maximum stress values and Young's modulus values

Sample No.	Carbon Fiber Volume Fraction (C_f)	Young's Modulus (GPa)
1C	0.1298	9.51
2C	0.1731	13.16
3C	0.2921	22.81
4C	0.3894	30
5C	0.4868	37.9
6C	0.5192	39.91
7C	0.7788	58.4

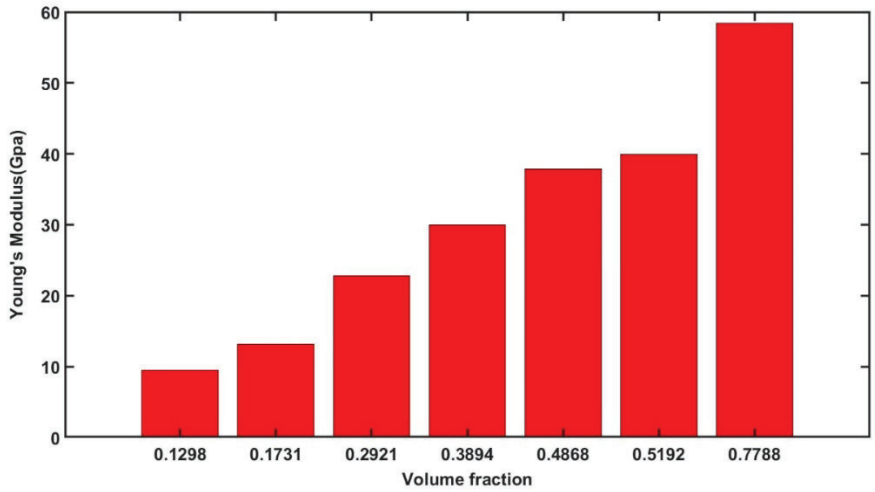

Figure 5. Increasing young's modulus with increasing volume fraction of specimens

Rule of Mixtures Model Development

The Rule of Mixtures (ROM) method is a simple approach to developing models for properties of composite materials. In this work, an ROM approach was employed, relying primarily on the extraction of a volume fraction for the fiber and the matrix. For ease of calculation and replicability of results, a MATLAB© application was developed to allow for the calculation of the fiber volume fraction. Figure 6 shows the interface of the developed application, and the result obtained when ran for the case of specimen 3C.

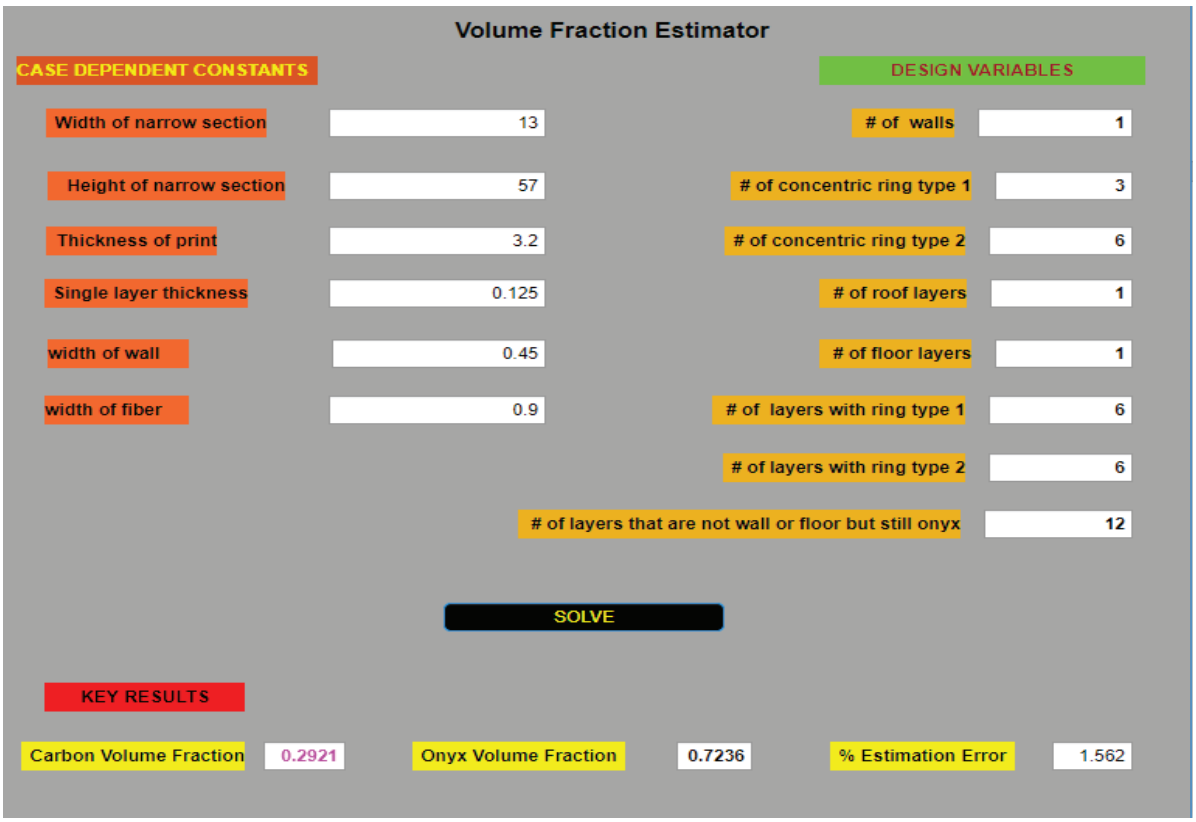

Figure 6. User interface of a MATLAB developed application for computation of volume fractions needed for the ROM model

Several parameters influence the calculation of the volume fraction for a specimen fabricated using the *Eiger* software discussed previously. All these parameters are provided in Table 3, with the equations that relate these parameters listed in Equations 1-9.

While the *Eiger* software provides values of total CCF and Onyx volume, this work is concerned specifically with the volume fraction in the gauge section. To do so, separate prints were fabricated and paused and removed from the printer for measurement, one such paused print is shown in Figure 7. A Keyence VR-3200 structured white light scanning microscope was used to measure the widths of the Onyx and the CCF, as shown in Figure 8. The layer thickness was 0.125mm (fixed setting), and the combination of the measurements and the known later thickness was used in the MATLAB application to estimate the volume fractions associated with each specimen, as discussed previously.

Table 3. Summary of measured parameters and relevant equation variables

Parameter	Interpretation	Value (mm)
W	Width of "reduced" section	13
T	Thickness of "reduced" section	3.2
H	Height of "reduced' section	57
T_{layer}	Thickness of single layer	0.125
W_{wall}	Width of wall	0.45
n_{wall}	Number of walls	Varies for each specimen
$N_{roofandfloor}$	Number of roof and floor layers	Varies for each specimen
W_{fiber}	Width of fiber	0.9
N_{fiber1}	Number of fiber layers with type 1 concentric rings	Varies for each specimen
n_{ring1}	Number of concentric fiber rings type 1	Varies for each specimen
N_{fiber2}	Number of fiber layers with type 2 concentric rings	Varies for each specimen
n_{ring2}	Number of concentric fiber rings type 2	Varies for each specimen
$N_{onyxonly}$	Number of layers in onyx only region (region that is not wall, or roof and floor, and not fiber region)	Varies for each specimen

$$V_{composite} = W \cdot H \cdot T \quad (1)$$

$$V_{roofandfloor} = 2\left[(W - 2W_{wall}n_{wall})HN_{roofandfloor}T_{layer}\right] \quad (2)$$

$$V_{wall} = 2W_{wall}T_{Layer}N_{Layer}Hn_{Walls} \quad (3)$$

$$V_{fiberregion} = \left(2W_{fiber}HN_{fiber1}T_{layer}n_{ring1}\right) + \left(2W_{fiber}HN_{fiber2}T_{layer}n_{ring2}\right) \quad (4)$$

$$V_{onyxinfiberregion} = T_L N_{fiber} H\left(W - 2W_{Walls}n_{walls} - V_{fiberregion}\right) \quad (5)$$

$$V_{onyxonlyregion} = (W - 2W_W n_W)T_L N_{onyxonly} \quad (6)$$

$$V_{matrix} = V_{onyxinfiberregion} + V_{roofandfloor} + V_{onyxonlyregion} \quad (7)$$

$$fiber\ volume\ fraction = \frac{V_{fiberregion}}{V_{composite}} \quad (8)$$

$$matrx\ volume\ fraction = \frac{V_{matrix}}{V_{composite}} \quad (9)$$

Figure 7. Cross section of a paused print showing the fiber region and onyx region

Figure 8. Cross section of a paused print showing relevant widths, as measured on a microscope

Given these specimens with varying volume fractions, and measured elastic moduli, the next step is to develop an ROM model with these values. Prior to so doing, the values and predictions were compared to supplier provided material data. Using Markforged's published material data with Tensile Modulus for Onyx and Carbon fiber being 1.4Gpa and 60Gpa respectively [7], and the estimated volume fraction values, Young's modulus values predictions were made and compared with experimentally obtained. Figure 9 shows good agreement at low fiber volume fractions but significant deviations at higher fiber volume fractions.

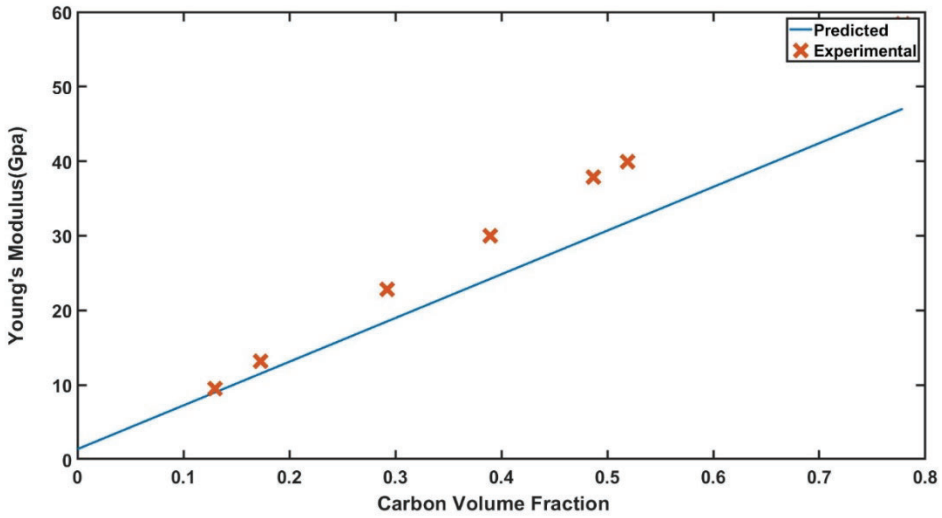

Figure 9. Young's modulus vs volume fraction using Mark forged published data when tensile properties of Onyx and Carbon fiber are used

Two different approaches were taken to develop the ROM model. The first was to extract Onyx modulus experimentally using the value obtained from the tensile test on the pure Onyx specimen (with no CCF). The CCF modulus was then obtained by using the experimental Onyx value and for each print specimen (1C-7C), individually solving for the CCF modulus. The values of the Carbon fiber moduli where then averaged and used to predict effective modulus that were

compared against already obtained experimental modulus. Using this approach, Figure 10 shows improved agreement between the model predictions and experimental results.

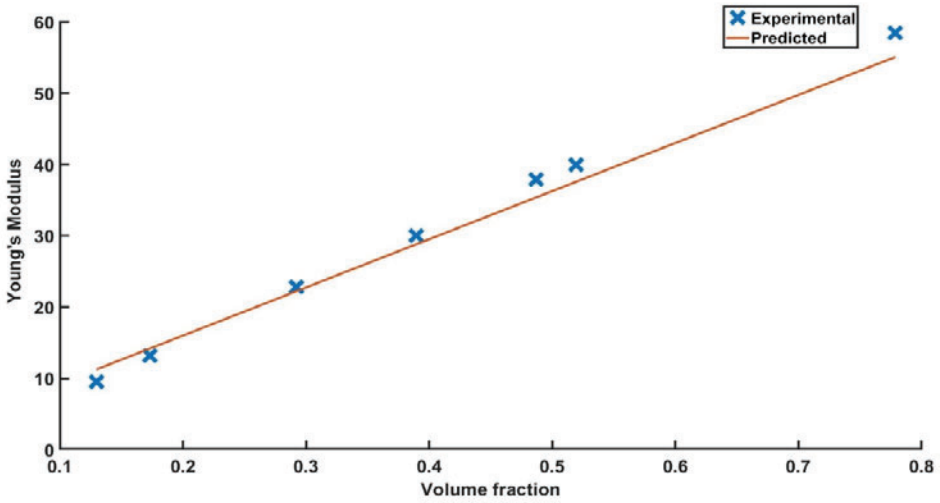

Figure 10. Young's Modulus vs Volume fraction of carbon when tensile values of Onyx and Carbon obtained experimentally ae used

Alternatively, the model may also be estimated using a linear fit of the experimentally obtained modulus values and solving the equation obtained from the fit (X=0, X=1) to obtain the moduli for CCF and Onyx as 75.9021 GPa and 0.3551 GPa respectively. This model, as is trivially expected from such an approach, shows good agreement generally throughout the range of fiber volume fraction values.

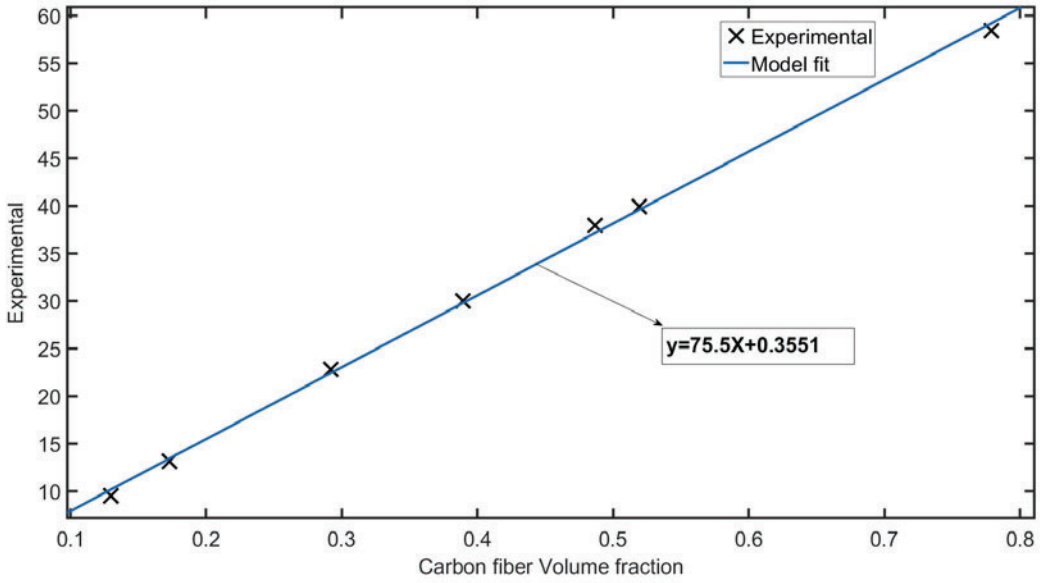

Figure 11. Linear fit of ROM model against experimental data

Applicability to Honeycomb Compression

To examine the validity of the ROM model developed in this work, honeycombs were fabricated on the same printer (MarkForged Mark Two) per the design shown in Figure 12a. The smallest thickness that could consistently fit two CCF paths within two walls of Onyx, as shown in Figure 12b was 3.72mm. A paused print with the CCF and Onyx visible is shown in Figure 12c.

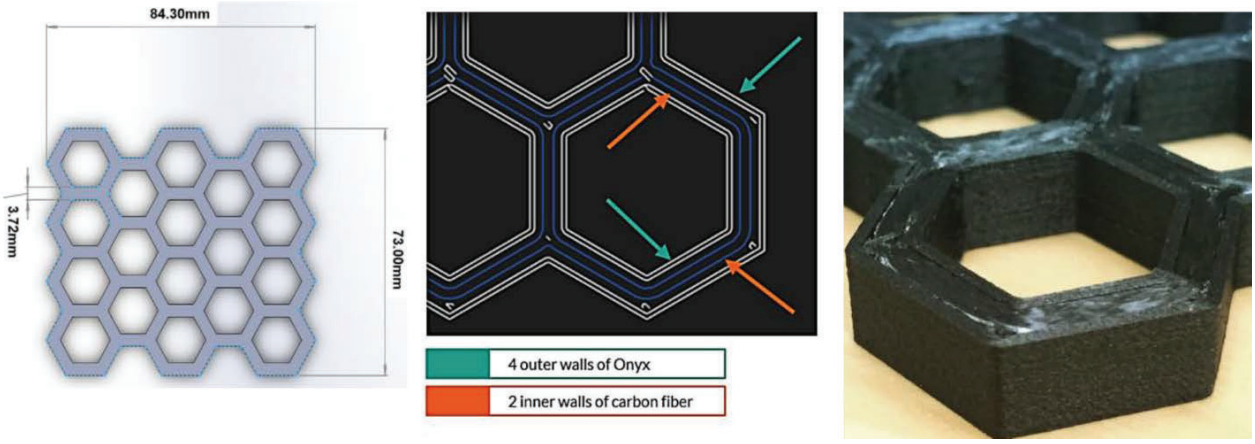

(a) (b) (c)

Figure 12. (a) CAD file of honeycomb with 3.72mm thick walls – this thickness was the minimum possible to (b) fit 2 inner walls of CCF within 2 walls of Onyx, (c) paused print showing the different paths of CCF and Onyx

These honeycombs were then subject to compression with an INSTRON 8801 (50kN load cell capacity). Initial data suggested a significant strain rate dependence (see Figure 13a) for both the effective modulus (Figure 14b) and for the peak load (Figure 13c). For this work, we are only concerned with the effective modulus, and as can be seen in Figure 13b, this value saturates below 10^{-3} s^{-1}.

The question of interest emerging from the prior work therefore was this: can the ROM model, when implemented in Finite Element Analysis (FEA) predict the response of the honeycomb under compression? To address this, material properties were required for the FEA model. With the prior ROM models, the only additional information needed is the volume fraction specific to the honeycomb beams. Once again, a paused print was measured with the Keyence microscope, as shown in Figure 14, and an average of measurements in 5 different regions was used to estimate a CCF volume fraction of 0.4773. Using the two ROM methods previously discussed, the elastic modulus was estimated as 36.41 and 34.71 GPa for the linear fit, and averaging methods, respectively.

The finite element model, developed in ANSYS, is shown in Figure 15b, and was setup with a mesh size such that 3 solid elements spanned the thickness of the beam – this was found to be sufficient from a refinement standpoint, in that subsequent refinement did not change reaction force results by more than 3%. The FEA model had frictional contacts between honeycomb and platen with a frictional coefficient of 0.15.

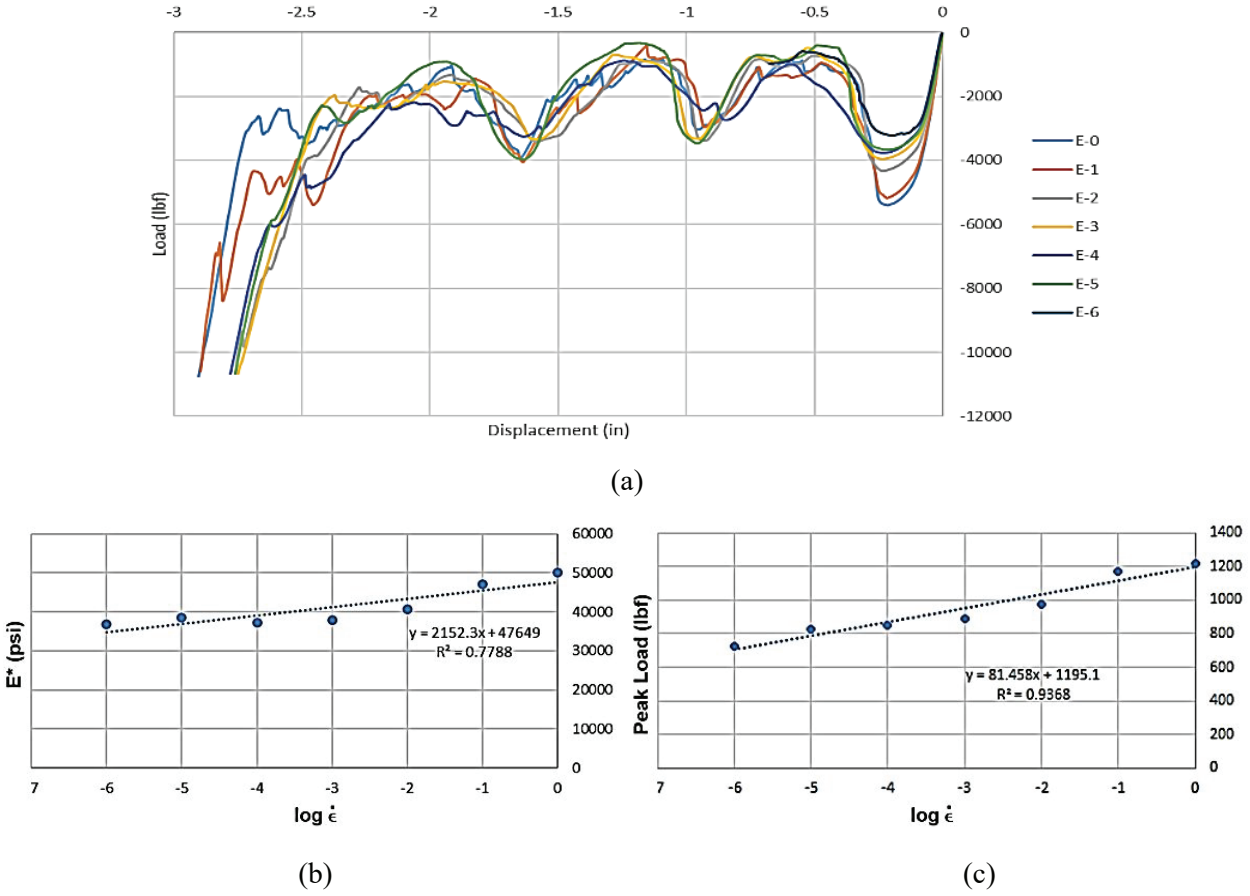

Figure 13. (a) Compression of honeycombs at effective strain rates spanning seven orders of magnitude, (b) effective elastic modulus, and (b) peak load (first maximum), as a function of effective strain rate

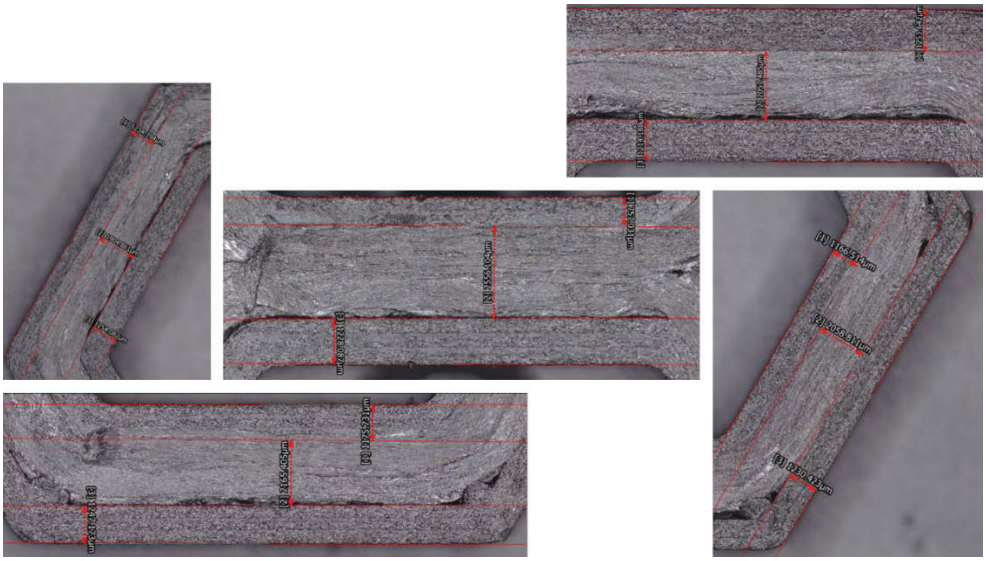

Figure 14. Measurements of Onyx and CCF widths for computation of volume fraction

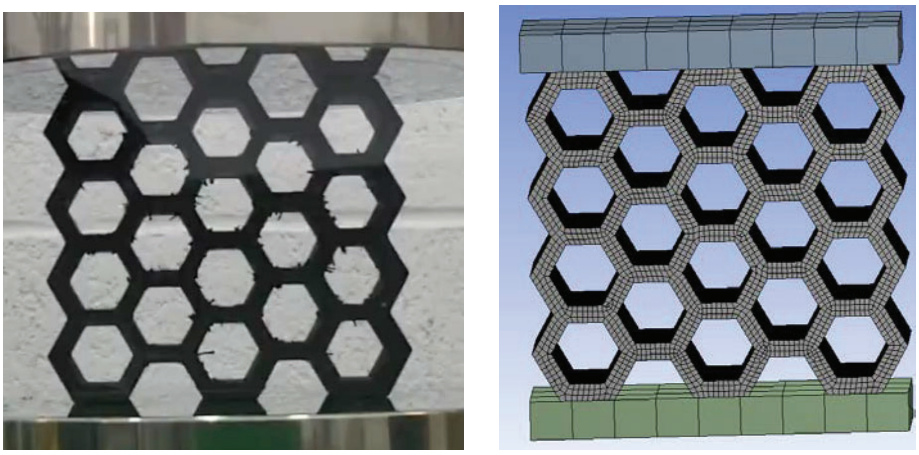

(a) (b)

Figure 15. (a) Experimental setup for honeycomb compression on an INSTRON 8801, and (b) FEA model simulating the same

Comparisons between the experimental result from the test conducted at 10-6 s-1, and the FEA model for both ROM approaches is shown in Figure 16. As can be seen the discrepancy is vast, with the experimental result vastly less stiff than that predicted in the model. This may be attributed to several reasons: the ROM model is derived from a pure tension study, with the fibers loaded only in the axial direction – in a honeycomb, in particular one as thick as this, the stress state is a combination of bending, axial and shear loading. A second contributing factor is the behavior at the nodes, which are idealized as having homogeneous properties, but in reality are the site of significant porosity, as seen in Figure 14. These results, while far from desired, are nonetheless presented here in the hope that they suggest future directions to the community concerned with modeling 3D printed composites.

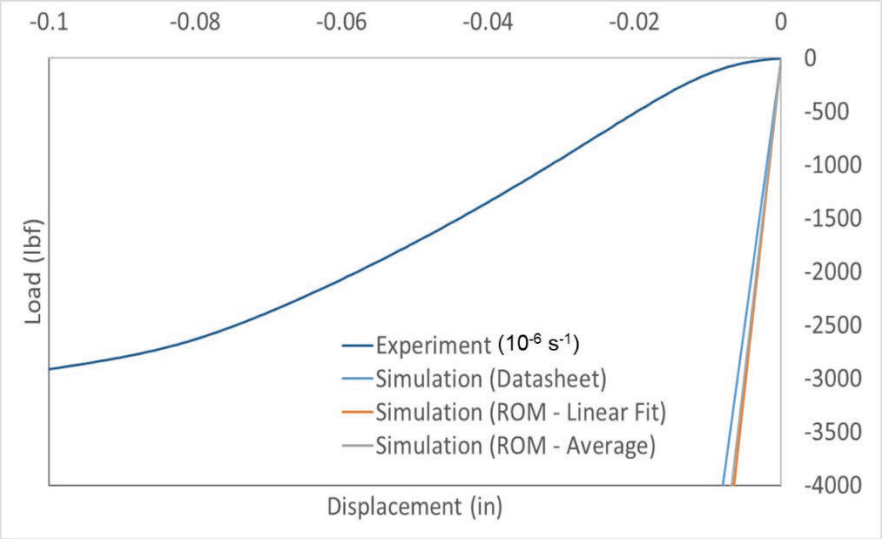

Figure 16. Comparison between FEA and experimental result showing a wide discrepancy

Discussion

This work adds to prior published work with regard to the development of ROM models for Continuous fiber composite 3D printing. The following three points are highlighted for discussion, and consideration in future work:

- The use of ASTM D638 specimen designs for composite 3D printing, as has been done by us in this work, and others in the literature, needs to be reexamined, with designs that are not sensitive to fiber start points and voids, developed.
- The large discrepancy between experimental and FEA modeling for the honeycomb compression indicates the need for a more thorough characterization effort beyond just tensile testing conducted here. Additionally, a more effective approach may be to characterize a member that matches the beam geometry and process parameters exactly [18] or extracts material properties using inverse homogenization approaches from testing honeycomb [19].
- Void regions are quite common in material extrusion based processes, and the composite 3D printing process used in this work is no exception. A more accurate model would therefore account for these voids.

Acknowledgements

This work was conducted as part of a research project in the MFG 598: Design for Additive Manufacturing course offered in the Spring of 2019 at the Arizona State University. The authors wish to acknowledge support from the Maricopa County Industrial Development Authority (MCIDA) and the Fulton Schools of Engineering at Arizona State University, where these parts were fabricated and tested.

References

1. Naranjo-Lozada, J., Ahuett-Garza, H., Orta-Castañón, P., Verbeeten, W. M., & Sáiz-González, D. (2019). Tensile properties and failure behavior of chopped and continuous carbon fiber composites produced by additive manufacturing. *Additive Manufacturing*, *26*, 227-241.
2. A.N. Dickson, J.N. Barry, K.A. McDonnell, D.P. Dowling, Fabrication of continuous carbon, glass and Kevlar fibre reinforced polymer composites using additive manufacturing,
3. Prüß, H., & Vietor, T. (2015). Design for fiber-reinforced additive manufacturing. *Journal of Mechanical Design*, *137*(11), 111409.
4. Ali, Hind & Alani, Tahseen & Othman, Farhad. (2018). Influence of Process Parameters on Mechanical Properties and Printing Time of FDM PLA Printed Parts Using Design of Experiment. 10.9790/9622-0807026569.

5. Jose F. Rodriguez, James P. Thomas, John E. Renaud, (2000) "Characterization of the mesostructure of fused-deposition acrylonitrile-butadiene-styrene materials", Rapid Prototyping Journal, Vol. 6 Issue: 3, pp.175-186, https://doi.org/10.1108/13552540010337056
6. Garrett W. Melenka, Benjamin K.O. Cheung, Jonathon S. Schofield, Michael R. Dawson, Jason P. Carey, Evaluation and prediction of the tensile properties of continuous fiber-reinforced 3D printed structures, Composite Structures, Volume 153, 2016, Pages 866-875, ISSN 0263-8223, https://doi.org/10.1016/j.compstruct.2016.07.018.
7. Forged, M. (2019). Retrieved 6 August 2019, fromhttp://static.markforged.com/downloads/composites-data-sheet.pdf Markforged. Markforged engineering grade thermoplastic. Available at: https://markforged.com/materials (2019).
8. 3DXTech, "Carbon Fiber Reinforced PLA Filament", (2014).
9. Ken-ichiro Mori, Tomoyoshi Maeno, Yuki Nakagawa, Dieless Forming of Carbon Fibre Reinforced Plastic Parts Using 3D Printer, Procedia Engineering, Volume 81, 2014, Pages 1595-1600, ISSN 1877-7058, https://doi.org/10.1016/j.proeng.2014.10.196.
10. ASTM D638–14, "Standard Test Method for Tensile Properties of Plastics", 2014.
11. Onyx Filament. (2019) Retrieved from https://markforged.com/materials/onyx/
12. Eiger (2019). Retrieved from https://markforged.com/eiger/
13. Instron: Fatigue Testing System - Model 8801 from Instron. (n.d.) Retrieved from https://www.azom.com/equipment-details.aspx?EquipID=1183)
14. The Mark two desktop 3D printer. (2019) Retrieved from https://markforged.com/mark-two/
15. Crease, A. (2016) Reinforcing 3D Printed Parts with Efficient Fiber Routing: Part 1. Retrieved from https://markforged.com/blog/reinforcing-3d-printed-parts-part-1/
16. Markforged. (2019) Retrieved from https://markforged.com/
17. Eiger Glossary (n.d.) Retrieved from https://support.markforged.com/hc/en-us/articles/115000260264-Eiger-Glossary
18. R. Sharma, T. Le, J. Song, E. Harms, D. Sowa, A, Grishin, D. Bhate, "A Comparison of Modeling Methods for Predicting the Elastic-Plastic Response of Additively Manufactured Honeycomb Structures," peer-reviewed proceedings, Solid Freeform Fabrication Symposium, 2018
19. T. Le, D. Bhate, J. Parsey, K. Hsu, "Determination of a Shape and Size Independent Material Modulus for Honeycomb Structures in Additive Manufacturing," peer-reviewed proceedings, Solid Freeform Fabrication Symposium, 2017